J. Innovative Eng. Nat. Sci., vol. 4, no. 2, pp. 326-353, 2024.
http://doi.org/10.61112/jiens.1397391

Araştırma Makalesi

Journal of Innovative Engineering and Natural Science
(Yenilikçi Mühendislik ve Doğa Bilimleri Dergisi)
https://dergipark.org.tr/en/pub/jiens

Parametric study on the assessment of the local buckling behavior of perforated square hollow sections with non-uniform wall thickness under axial compression

Mehmet Akif Dundar [a,*] Mirali Nuraliyev [a,*]

[a] *Yozgat Bozok University, College of Engineering, Mechanical Engineering Department, 66100, Yozgat/Turkey.*

ARTICLE INFO

Article history:
Received 28 Nov 2023
Received in revised form 17 Jan 2023
Accepted 3 Feb 2023

Available online

Keywords:
Local stability
Square hollow section (SHS)
Circular web openings
Perforations
Axial compression
Local buckling coefficients
Finite element analysis

ABSTRACT

The aim of this rigorous parametric study is to explore the influence of perforations on the local buckling behavior of square hollow sections (SHSs) possessing non-uniform wall thickness. A finite element procedure followed in the current study has been first validated against existing test results documented for the local buckling behavior of the perforated SHS with uniform web and flange segment thickness under axial compression. The linear elastic eigenvalue buckling and elastoplastic buckling analyses have been implemented using the Abaqus engineering finite element code. The verification of the numerical procedure has been achieved by favorably comparing the finite element results with the existing test results in terms of the first local buckling mode shape and load-end shortening curves of the perforated SHS with uniform wall thickness. . The verified numerical procedure has been applied to the problem of finding the perforation effect on the local buckling response of the SHS with non-uniform thickness. Finite element analyses have been performed for four various web width-to-perforation diameter ratios ranging from 0.3 to 0.9. Finite element analysis results have revealed that the presence of perforations does not influence the local buckling mode shape of the SHS but considerably affects the critical local buckling loads. The results have put forth that increasing perforation diameter leads to a more pronounced and drastic decrease in the critical local buckling load. The outcomes of the study have also shown that the critical post-buckling load of the SHS with non-uniform wall thickness is less susceptible to perforations compared to the SHS with uniform wall thickness. The results obtained in the context of this parametric study have been made available to practical engineering for use in actual design of the perforated SHSs.

I. INTRODUCTION

Square hollow sections (SHSs) have been receiving a great deal of attention for use as load-carrying components in a broad range of application fields, including construction and automotive, due to their many promising mechanical advantages over solid sections, such as a higher strength-to-weight ratio [1–6]. This important mechanical quality offered by SHSs makes them very ideal for use in specific applications where high strength with low weight is required [7]. As with other hollow section members possessing different section shapes including rectangular and circular, understanding their failure mechanism under loads is highly imperative for reliable design. The robust design of SHSs is generally achieved by considering both adequate- strength and local stability requirements in a balanced way [8–11]. Taking into account the adequate-strength criterion alone can lead the SHS to suffer local buckling prior to reaching its maximum load-carrying capacity, which brings additional material cost [8, 12]. In other words, a critical elastic local buckling load of the SHS needs to be considered its collapse load since the SHS cannot sustain any additional load after undergoing local elastic buckling [13–15].

*Corresponding Author: Tel: +90-544-463-4075, e-mail: m.akif.dundar@yobu.edu.tr

The use of cold-formed steel SHSs as primary load-carrying components in numerous application fields has been increasing steeply due to their high strength and high stiffness -to- weight ratios compared to hot-formed SHSs [3, 16–19]. The key point of the local stability-based design of cold-formed steel SHSs is to first understand the influence of the cold-forming process on material attributes and then to reproduce their non-linear stress-strain curves by using a suitable material model [1, 3, 20, 21]. In general, cold-forming leads to a considerable increase in the yield and ultimate strengths of the steel but a significant decrease in its ductility [3, 5, 22–24]. Especially, the corner segments of SHSs undergo extremely large plastic deformations due to their constricted corner radius during the cold-forming process. This larger plastic deformation results in higher yield and ultimate strengths with less ductility in comparison in the corner coupons in comparison with the flat coupons of SHSs [3, 5, 25, 26]. Up to the present time, a considerable number of material models have been developed to describe the non-linear stress-strain behaviors of cold-formed steels [3, 27–29]. Among them, a constitutive expression developed by Ramberg and Osgood [27] is considered the most notable material model to specify the mechanical characteristics of cold-formed steels.

As reported by a significant number of researchers, thin-walled cold-formed SHSs are susceptible to global and local elastic buckling as well as post-buckling [30–32]. This is mainly due to the inherent weakness of the thin-walled SHS [30]. Beyond this inherent weakness, their sophisticated local buckling failure modes induced by different loading configurations, like axial compression, bending, and combined axial compression and bending make their satisfactory prediction of the local buckling and post-buckling behaviors very difficult [30]. American Iron and Steel Institute's Direct Strength Method (DSM) and Finite Strip Model (FSM) are the two common approaches that take into account the local elastic buckling properties for the specification of the local stability limit of the thin-walled structural members [14, 32–35]. In order to calculate the critical local elastic buckling stress of the box sections with uniform wall thickness, analytical expressions defining the local buckling coefficients have been developed and reported for the different cross-section dimensions (width-to-height ratio) and different loading configurations including axial compression, bending, biaxial bending and combined axial compression and bending [14, 15, 35]. One of the most notable studies has also documented the local buckling mode shapes of the box sections for various types of loads [14]. Note that the local buckling coefficients and local buckling mode shapes reported are valid for the box sections possessing uniform thickness. Interestingly, the lack of analytical expression that describes the local buckling coefficients of SHS with non-uniform wall segment thickness for specific loading configurations such as major axis bending, minor axis bending, and bi-axial bending makes finite element analyses a powerful tool to deal with these types of unique local stability problems. For the axial compression loading case, only one exploratory study has reported the local buckling coefficients of SHS possessing different web and flange thicknesses [36]. Apart from the inexistence of an analytical solution for the calculation of local buckling coefficients of SHSs with unequal wall thickness, perforations can sometimes be placed on SHSs for connection or aesthetic purposes, which makes their local stability analysis more difficult in terms of theoretical aspects [26, 32, 37]. In other words, none of the aforementioned models (DSM and FSM) can explicitly handle the imperfections or discontinuities induced by perforations [37]. In this case, finite element analyses need to be applied to the problem of solving the local buckling behaviors of the perforated SHSs [26, 32, 37]. A finite element analysis is very useful for local buckling studies involving geometric imperfections caused by holes.

Considerable attention has been paid to comprehending the impact of imperfections generated by cut-out holes, cracks, damage, and delamination on the mechanical behaviors of various types of materials such as metal, composites, and functionally graded materials (FGMs) [38–42]. From those studies, it has been deduced that the numerical modeling of the formations of geometric imperfections in composites and FGMs is a harder task than the metallic materials due to their non-symmetrical property variations [39, 41] and this research topic still attracts great attention.

In essence, a deep understanding of the local buckling and post-buckling behavior of SHSs as well as comprehending the perforations effect on their local stability is of great importance to the industry in terms of material savings. In order to gain a deep insight into the circular perforation effect on the local buckling behavior of rectangular plates from which SHS are constituted, a considerable number of exploratory studies have been dedicated so far [43–47]. Those studies have reported that the local stability of the rectangular plates is adversely influenced by the presence of circular perforations, and this unfavorable effect becomes more evident with increasing circular perforation diameter. Parametric studies carried out on the perforated plates have concluded that a decrease observed in the critical local buckling load is mainly due to the weakened cross-section of the plates resulting from the circular openings [48–50].One of the most noteworthy outcomes has also been reported that the critical local buckling stress might enhance with increasing the circular opening diameter beyond a certain limit as a result of the redistribution of stresses in the plates [48–50]. Furthermore, a notable finite element study has put forth that the plate with a circular perforation offers a higher critical local buckling load than the plate with a square perforation [51]. Aside from the perforated plates, the effects of perforations possessing different shapes (circular, square, or rectangular) on the local buckling behavior of thin-walled structures with different shapes (circular, rectangular, and square) have been examined [52–57]. A notable parametric study has focused on investigating the effects of cut-outs with different shapes, including square, rectangular, and circular on the local buckling behavior of an axially-loaded circular tube [53]. In addition to the mentioned perforation shapes, the location of the holes and the number of holes have been assessed employing finite element analyses [53]. This study has shown that the local buckling failure mode of the circular tube is independent of the shape perforation. It has also been concluded that the cylindrical thin-walled tube with a circular perforation of a diameter identical to the width of the square cut-out sustains a similar buckling load before collapse [53].The study has also revealed that the critical local buckling load of the circular thin-walled tube decreases with increasing perforations size and the number of perforations but is not affected pronouncedly by the location of perforations in the structure [53]. Similar results related to the effect of perforation location have also been reported by a comprehensive parametric study carried out on cold-formed SHS with equal wall segment thickness under axial compression [26]. Albeit a higher local buckling strength offered by the hot-formed SHS under axial compression, paying the larger price for the hot-formed SHS compared to its equivalent cold-formed SHS negates the advantage of the hot-formed SHS in terms of local buckling resistance [58]. Opposite to the parametric studies [26, 53], a parametric study centered on examining the impact of a single circular opening on the local buckling behavior of the circular tube, made of a lean duplex stainless steel, has shown that the location of the opening has a considerable influence on the local buckling load and a maximum decrease in the local buckling load of the circular tube takes place when the single circular opening is located at mid-height of the structure [57]. Nevertheless, in contrast to the circular thin-walled tube, a square cut-out impairs the local buckling load capacity of SHS more severely than the hexagon and circular perforations of the

same size [26]. The effect of the presence of perforations on the local buckling behavior of the lipped channel section on the local has been studied by performing parametric studies [55].

The literature review documented above clearly indicates that the parametric studies primarily focused on examining the local buckling behavior of perforated plates and circular thin-walled tubes. A few parametric studies have attempted to provide a better understanding of the effect of circular perforations on the local buckling parameters of the cold-formed SHS subject to axial compression, including the critical local buckling load and local buckling failure mode. Nevertheless, the parametric studies carried out on the cold-formed SHS are limited to the SHSs with equal wall segment thickness. In the literature, there is a lack of parametric studies addressing the effect of circular perforations on the local buckling behavior of SHSs with unequal wall segment thicknesses.

In order to fill the above deficiency noticed in the literature, this parametric study has been thereby devoted to endeavoring the circular perforation effect on the local buckling behavior of cold-formed SHS with unequal wall thickness subject to axial compression through finite element analyses. To this end, finite element analyses have been implemented using the Abaqus engineering finite element software. Two various finite element analyses including linear elastic eigenvalue and post-buckling have been performed on the perforated SHS. Local buckling failure modes extracted from the linear elastic eigenvalue buckling simulations have been successfully introduced to the finite element model of the post-buckling. Results obtained from the numerical analysis have been clearly presented and well-documented. In essence, this study actually has explored the perforation effects on the local stability performance of the SHS with non-uniform wall thickness for the first time.

II. THEORETICAL BACKGROUND

In the case of the square hollow section (SHS) illustrated in Fig.1, an associated local buckling mode is obtained without displacements of the adjacent of the web and flange segments [14, 15]. In other words, the influence of rotational constraints provided by the adjacent walls is not taken into account in calculating the local buckling stress. This actually signifies that each wall segment can suffer from buckling independently. The calculation of the critical stress for local instability involves the geometric dimensions of SHS, material properties, and local buckling coefficients.

In terms of geometric dimensions, elastic material properties, and local buckling coefficient, the critical stress for local instability can be described as follows [14, 15]:

$$\sigma_{cr}=k_{\sigma}\frac{\pi^2 E}{12(1-v)^2}\left(\frac{t}{b}\right)^2 \quad (1)$$

where σ_{cr} is the critical local buckling stress. E and v represents the elastic modulus and Poisson's ratio, respectively. t and b are the associated flange or web thickness and its thickness, respectively.

Assuming that the critical buckling stress at the mid-points of the web and flange adjacent is equal, the expression given in Eq. (1) can be rearranged as given below.

$$\sigma_{cr}=k_w \frac{\pi^2 E}{12(1-v)^2}\left(\frac{t_w}{h_w}\right)^2=k_f \frac{\pi^2 E}{12(1-v)^2}\left(\frac{t_f}{b_f}\right)^2 \quad (2)$$

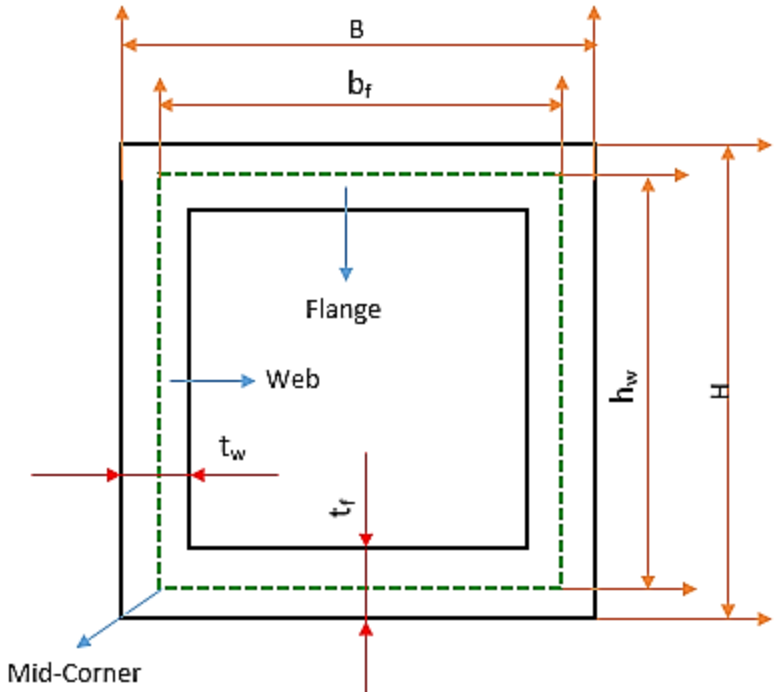

Figure 1. Cross-section of SHS with uniform flange and web thickness

Herein, k_w and k_f denote the local buckling coefficient for the web and flange, respectively. Note that these local buckling coefficients vary significantly based on the geometric dimensions of SHS as well as a loading configuration.

The thickness of flange and web segments is represented by t_w and t_f, respectively. The parameters of h_w and b_f can be computed using the following expressions.

$$h_w=\text{H-}t_f \quad (3)$$

$$b_f=\text{B-}t_w \quad (4)$$

where t_w and t_f are the web and flange thickness, respectively. H and B denote the web width and flange width, respectively.

When the web thickness is equal to the flange thickness ($t_f = t_w$), the relation between k_w and k_f can readily be extracted from Eq. (1) as given below.

$$k_f = k_w(\frac{b_f}{h_w})^2 \quad (5)$$

In the case of SHS with a uniform thickness, it is known that b_f is equal to h_w ($b_f = h_w$), leading to

$$k_f = k_w \quad (6)$$

The expression presented in Eq.(6) signifies that the local buckling coefficient of web is equal to the local buckling coefficient of flange in the case of SHS possessing uniform wall thickness. However, it is important to underline that the local buckling coefficient differ from a loading configuration to a loading configuration [14, 15, 35]. For the axial compression loading configuration, it is very well known that both k_w and k_f are equal to 4 [14, 35].

If the SHS does not possess the identical wall thickness, Eq. (5) can be rewritten accordingly as given below.

$$k_f = \frac{k_w}{(\frac{t_f}{t_w})^2} \quad (7)$$

It is worth emphasizing that the local buckling coefficients for SHS with non-uniform wall thickness have never been reported for the bending loading configuration but they have been made available by the study for use in design applications for the axial compression loading [36].The buckling mode of SHS possessing uniform wall thickness has been reported for the axial compression case as depicted in Fig.2 but the buckling mode of SHS with non-uniform thickness has never been presented for any loading configuration to date.

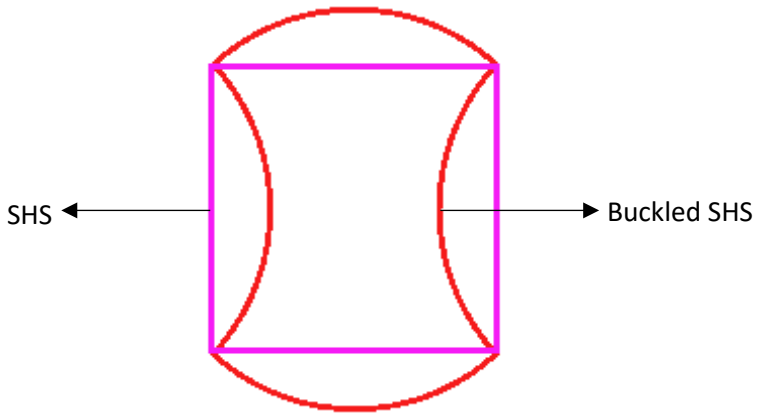

Figure 2. Buckling mode of SHS with uniform wall thickness under axial compression [14]

III. PROBLEM DESCRIPTION

The local buckling problem of the perforated SHS under axial compression addressed to validate the finite element procedure followed in this study is clearly depicted in Fig.3. The local buckling performance of the perforated SHS made of cold-formed YST-310 steel has been explored by conducting axial compression tests. During the mechanical tests, one end of the SHS was fixed and the other end was allowed to move in the loading direction. A detailed description of the experimental setup can be found in the relevant study [26]. The axial compression tests have been conducted of the perforated SHS for three various web width-to-perforation diameter ratios (d/w) ranging from 0.5 to 0.9. During the mechanical tests, load and corresponding end-shortening curves were successfully measured and well documented in the associated study [26]. The complete geometrical specifications of the perforated SHS is tabulated in Table 1.

Table 1. The complete geometrical specifications of the perforated SHS [26, 59]

Cross-Section	B (mm)	t_w=t_f (mm)	L (mm)	r_i (mm)	r_o (mm)	w (mm)	d (mm)	d/w
50x50x2.9d/w0.5	50	2.9	200	2.9	5.8	38.4	19.2	0.5
50x50x2.9d/w0.7	50	2.9	200	2.9	5.8	38.4	26.9	0.7
50x50x2.9d/w0.9	50	2.9	200	2.9	5.8	38.4	34.6	0.9

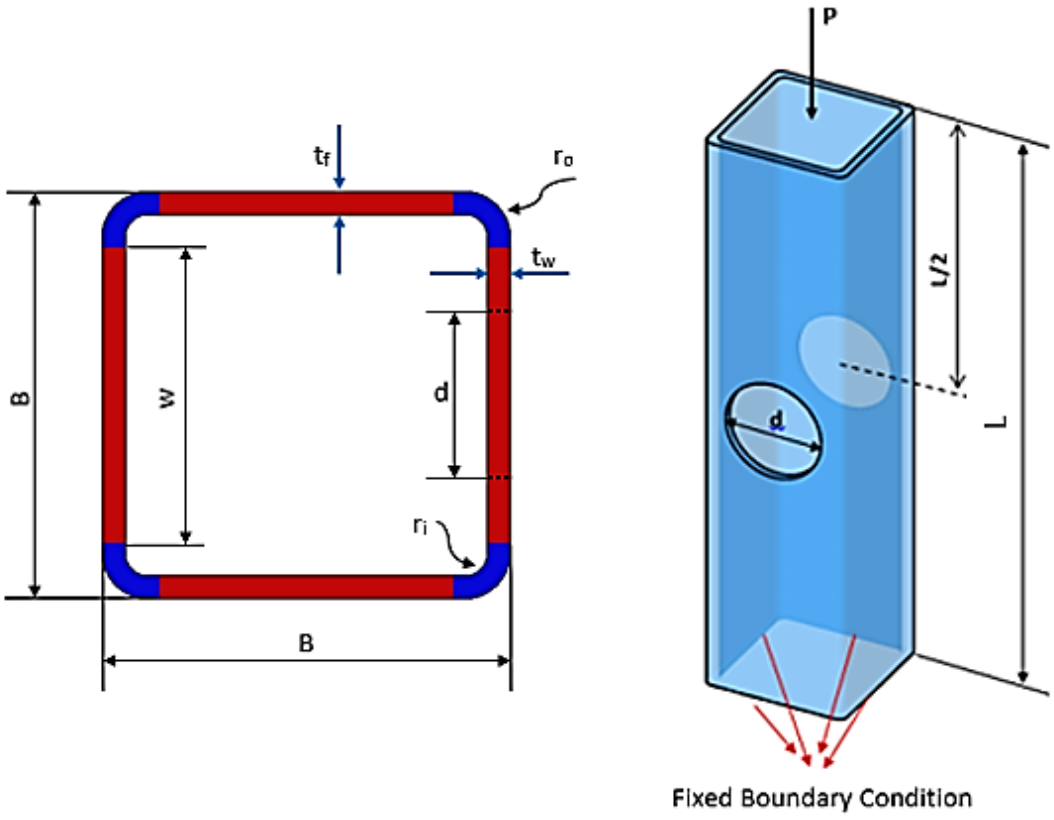

Figure 3. The local buckling problem of the perforated SHS addressed for validation [26]

IV. VALIDATION OF THE FINITE ELEMENT PROCEDURE AND RESULTS

A finite element method has been applied to the problem of predicting the local buckling behavior of the perforated and unperforated SHSs subject to axial compression. Finite element analyses have been implemented using the Abaqus finite element engineering software. Two distinct finite element analyses including linear elastic eigenvalue and elastoplastic, have been performed on the SHS. The first local buckling mode shape extracted from the linear elastic eigenvalue buckling analysis has been introduced as a geometric imperfection to the finite element model of the elastoplastic buckling analysis. The finite element model of the local buckling problem shown in Fig.3 is illustrated in Fig.4. The grid geometry of the SHS has been meshed using the 3-dimensional continuous eight-node element with reduced integration designated C3D8R in Abaqus [60]. The capability of this element type to predict the local buckling behavior of structures has been reported by many studies [61–64]. After studying mesh convergence, an average number of 33600 C3D8R elements have been decided to use in numerical simulations.

As depicted in Fig.4, two reference points have been defined at the geometric centers of both ends and these reference points have been linked to the SHS through kinematic couplings [8, 26, 65]. Boundary conditions and axial load transferred to the SHS by means of the defined kinematic couplings have been imposed on the reference points. While one end of the SHS has been fixed in all directions, the other end has been allowed to move in the loading direction as shown in Fig.4. In order to improve the computational accuracy, the region of the SHS near perforations has been meshed finer than its remaining region.

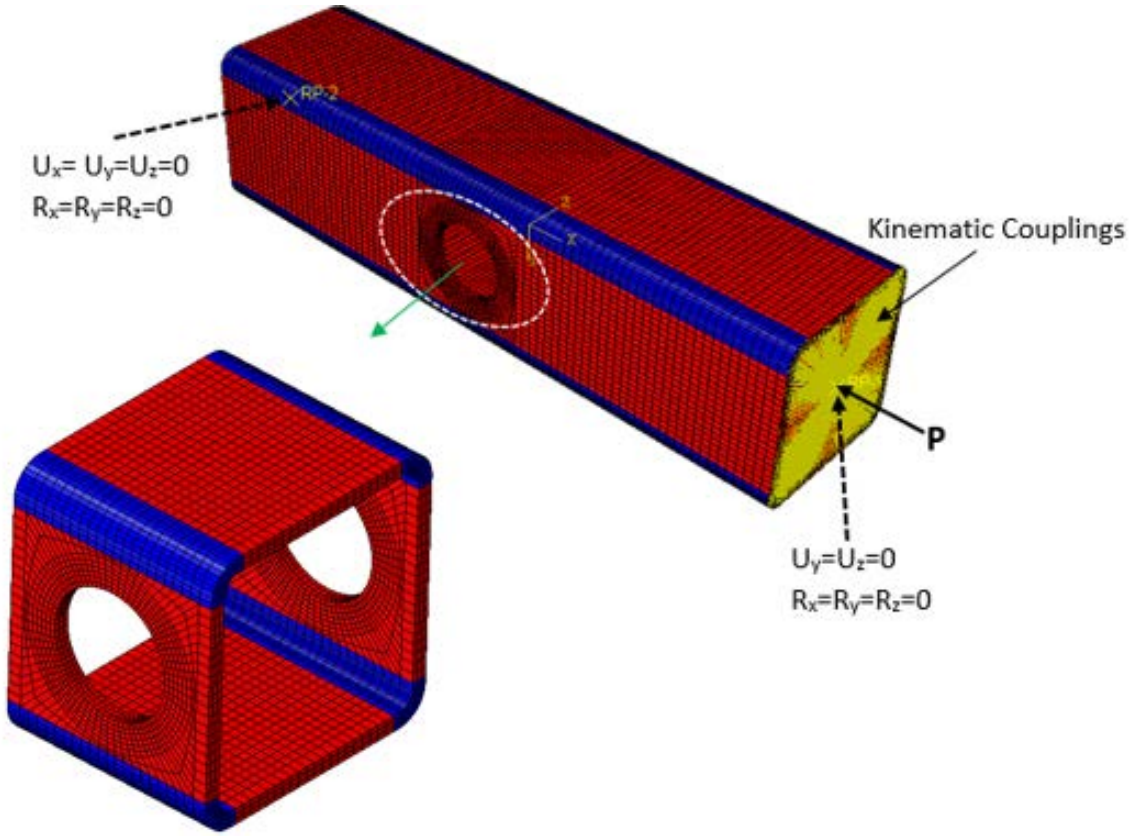

Figure 4. The finite element model of the perforated SHS

In accordance with the studies presented in the relevant literature [5, 8, 26, 65–67], non-linear buckling analyses have been performed using the RIKS method offered by Abaqus. The geometric imperfections obtained from the linear eigenvalue elastic buckling analysis have been successfully incorporated into the finite element model of the non-linear buckling analysis (RIKS). During the non-linear buckling analysis, the axial load has been increased gradually. It is worth stating that the lowest local buckling mode shape has been achieved using the Lanczos eigensolver available in Abaqus. In a consistent manner, the amplitude of local imperfection has been set to t/100 in the non-linear buckling analysis [26].

As mentioned earlier, a cold-forming process plays a significant role in the material properties of steel. For the corner coupon and flat coupon of the SHS made of cold-formed YSt-310 steel, the material properties taken from the associated study are tabulated in Table 2.

Table 2. Material properties of the flat and corner coupons of the SHS made of YSt-310 [5, 26]

Region	E (MPa)	σ_y (MPa)	σ_u (MPa)	ε_f (%)	n
Flat Coupon	190024	370	446.48	22.56	4.2
Corner Coupon	176191	506	571.53	7.69	2.7

In Table 2, E represents the Young's modulus. σ_y and σ_u denote the yield strength and ultimate strength, respectively. ε_f and n are the fracture strain and a strain hardening exponent, respectively. Note that σ_y is determined by using the 0.2% offset method.

To describe the mechanical behaviors of the flat and corner coupons of the SHS in the numerical simulations, their engineering stress-strain curves have been regenerated using the following expressions developed by Ramberg-Osgood[27].

$$\varepsilon = \frac{\sigma}{E} + 0.002\left(\frac{\sigma}{\sigma_y}\right)^n \quad , \qquad 0 < \sigma \leq \sigma_y \tag{8}$$

$$\varepsilon = \frac{\sigma - \sigma_y}{E_{0,2}} + \left(\varepsilon_u - \varepsilon_{0,2} - \frac{\sigma_u - \sigma_y}{E_{0,2}}\right)\left(\left(\frac{\sigma - \sigma_y}{\sigma_u - \sigma_y}\right)^m\right) \quad , \qquad \sigma > \sigma_y \tag{9}$$

where $E_{0,2}$ is known as the tangent modulus and can be computed using the following expression [3].

$$E_{0,2} = \frac{E}{1 + 0.002n\left(\frac{E}{\sigma_y}\right)} \tag{10}$$

Furthermore, m is the second strain hardening exponent that can be defined for the current case as follows:

$$m = 1 + 2.8(\frac{\sigma_y}{\sigma_u}) \tag{11}$$

Finally, the ultimate strain ε_u can be defined as given below[3].

$$\varepsilon_u = 0.6(1 - \frac{\sigma_y}{\sigma_u}) \tag{12}$$

Note that the expression given in Eq. (12) is only valid for the flat coupon. The ultimate strain of the corner coupon has been registered from the given engineering stress-strain curve [5].

After reproducing the engineering stress-strain curves by using the above expressions, they have been converted into the true stress-strain curves by using the well-known relations below.

$$\sigma_T = \sigma_{eng}(1 + \varepsilon_{eng}) \tag{13}$$

$$\varepsilon_T = ln(1 + \varepsilon_{eng}) \tag{14}$$

Herein, σ_T is the true stress and ε_T is the corresponding true strain. In the same manner, σ_{eng} is the engineering stress and ε_{eng} is the corresponding engineering strain.

In order to define the mechanical behaviors of the flat and corner coupons in the finite element analysis, a deformation plasticity model developed based on the Ramberg-Osgood model has been taken into account [68]. An entire stress-strain curve of the work material can be produced by the deformation plasticity model that is generally applicable to the fully plastic analysis of ductile metals.

For the one dimensional case, the deformation plasticity theory is defined as given below.

$$E\varepsilon = \sigma + \alpha(\frac{|\sigma|}{\sigma_y})^{(n-1)} . \sigma \tag{15}$$

where σ is the stress and n is the hardening exponent. α represents the yield offset and can be described as follows:

$$\alpha = \frac{E\varepsilon}{\sigma_y} - 1 \tag{16}$$

The deformation plasticity material model parameters calculated for the flat and corner sections of the SHS are documented in Table 3.

Table 3. The deformation plasticity material model parameters calculated for the flat and corner sections

Region	E (MPa)	σ_y (MPa)	α	n
Flat Coupon	190024	370	1.025	13.84
Corner Coupon	176191	506	0.68	8.4

Using Eq. (15) as well as the defined parameters in Table 3, the true stress-strain curves of both coupons have been produced and compared to experimental results, as given in Fig.5 and Fig.6. In essence, the experimental true stress-strain curves of the flat and corner coupons have been reproduced very satisfactorily by the deformation plasticity model; therefore, the parameters documented in Table 3 have been used to determine the mechanical behaviors of both coupons in numerical simulations.

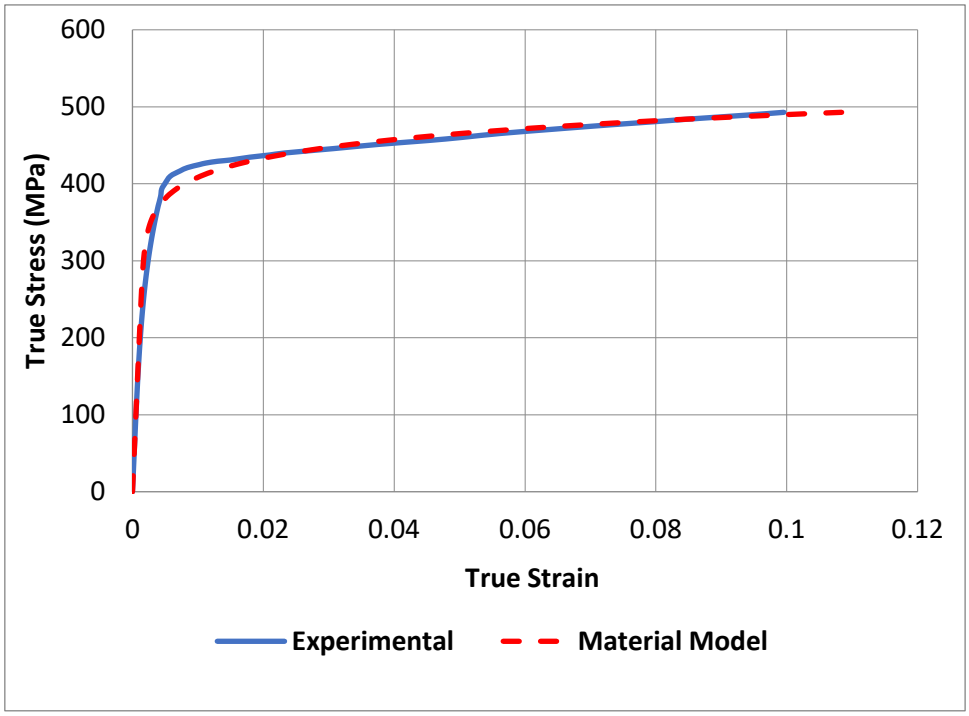

Figure 5. The true stress-strain curve of the flat coupon

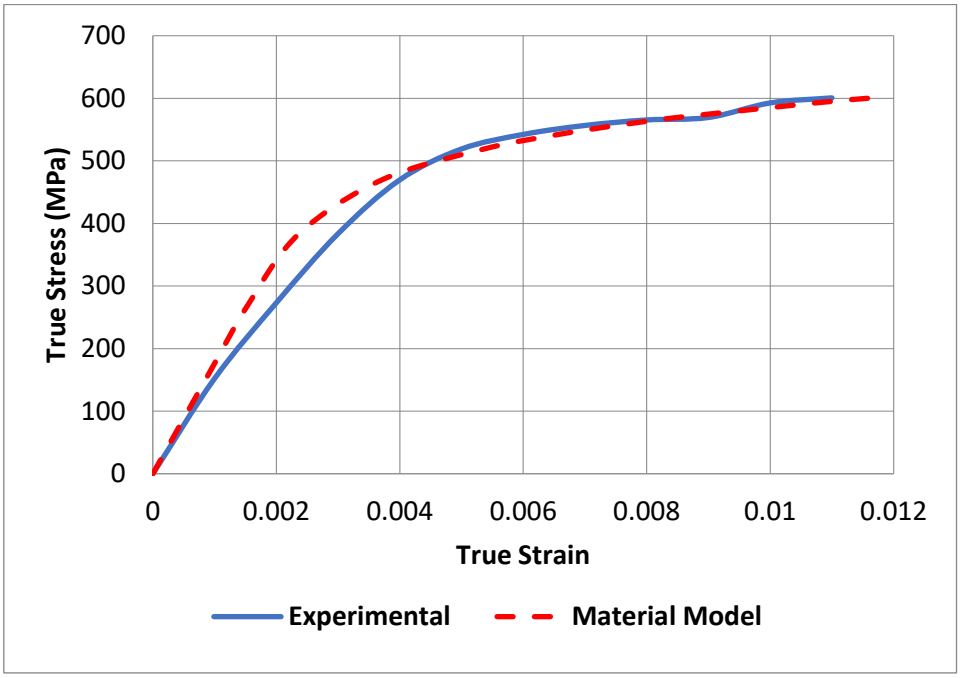

Figure 6. The true stress-strain curve of the corner coupon

The first local buckling mode shape and corresponding critical buckling load of the unperforated SHS extracted from the linear elastic eigenvalue buckling analysis are illustrated in Fig.7.

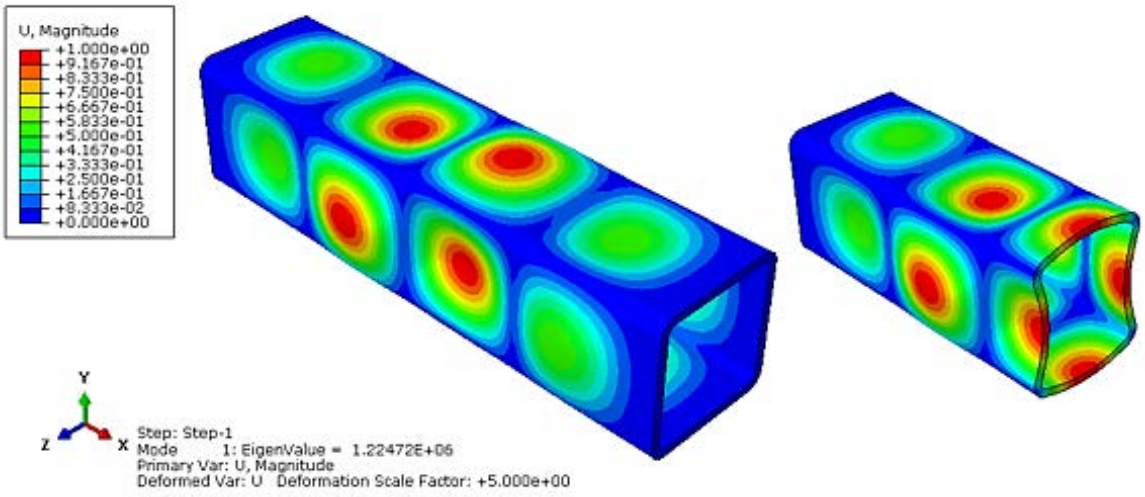

Figure 7. The first local buckling mode shape of the unperforated SHS under axial compression

One important outcome deduced from the results in Fig.7 is that the predicted mode shape is consistent with the theoretically derived mode shape presented in Fig.2. For this case, the critical local buckling load has been predicted to be 1.224×10^6 N. Since the SHS addressed, in this case, is unperforated, calculating its critical local buckling stress and therefore critical local buckling load by using Eq.(2) is possible. Nevertheless, only one Young's modulus appears in Eq. (2) but the flat coupon and corner coupon possess dissimilar Young's modulus as documented in Table 3. To eradicate this issue, an expression to compute an effective Young's modulus has been derived as follows:

The total force, P, acting on the entire cross-section of the SHS can be defined as given below.

$$P = P_f + P_c \tag{17}$$

where P_f and P_c are the acting axial loads on the flat and corner coupons, respectively.

In terms of stress, Eq. (17) can further be rearranged as given below.

$$\sigma_{eff}.A_g = \sigma_f.A_f + \sigma_c.A_c \tag{18}$$

Herein, A_g is the gross-sectional area of the SHS. A_f and A_c are the section area of the flat and corner coupons, respectively.

Dividing both sides of the Eq.(18) with A_g leads to the following relation.

$$\sigma_{eff} = \sigma_f.\frac{A_f}{A_g} + \sigma_c.\frac{A_c}{A_g} \tag{19}$$

The quantities of $\frac{A_f}{A_g}$ and $\frac{A_c}{A_g}$ actually imply the flat coupon area fraction and corner coupon area fraction, respectively.

Defining $v_f = \frac{A_f}{A_g}$ and $v_c = \frac{A_c}{A_g}$ yield the following expression.

$$\sigma_{eff} = \sigma_f.v_f + \sigma_c.v_c \tag{20}$$

Note that $v_f + v_c$=1.

Taking into account the well-known relation, the expression given in Eq. (20) can be rewritten as follows:

$$E_{eff}.\varepsilon = E_f.v_f.\varepsilon_f + E_c.v_c.\varepsilon_c \quad (21)$$

where ε is the total strain. $\varepsilon_f and\ \varepsilon_c$ are the strains sustained by flange coupon and corner coupon, respectively. Furthermore, E_{eff} denotes the effective Young's modulus and $E_f\ and\ E_c$ are the Young's modulus of flat coupon and corner coupon, respectively. Knowing that $\varepsilon = \varepsilon_f = \varepsilon_c$ in the case of axial loading, the expression given in Eq. (21) reduces to

$$E_{eff} = E_f.v_f + E_c.v_c \quad (22)$$

For the current case, $A_g = 524.7\ mm^2$, $A_f = 445.44\ mm^2$ and $A_c = 79.26\ mm^2$ which leads to $v_f = 0.85$ and $v_c = 0.15$.

The effective modulus can readily be calculated as given below.

$$E_{eff} = 190024x0.85 + 176191x0.1 = 187949\ MPa \quad (23)$$

In terms of E_{eff}, Eq.(2) can be rearranged as given below.

$$\sigma_{cr}=k_w \frac{\pi^2 E_{eff}}{12(1-v)^2}\left(\frac{t_w}{h_w}\right)^2=k_f \frac{\pi^2 E_{eff}}{12(1-v)^2}\left(\frac{t_f}{b_f}\right)^2 \quad (24)$$

As reported previously, $k_w = k_f = 4$, $t_w = 2.9\ mm$ (Table 1) and $h_w = 47.1\ mm$.

Substituting the above quantities into Eq.(24) leads to $\sigma_{cr} = 2573\ MPa$. The critical local buckling load can be computed using the following expression.

$P_{cr} = \sigma_{cr} x\ A_g$=2573x524.7=1.35x10^6 N (25)

The critical local buckling load has been predicted to be 1.224x10^6 N by the finite element analysis. The error ratio between numerical and theoretical results has found to be 9.3%. This relatively high error ratio can be attributed to the neglect of the effect of round corners in the theoretical calculations. In essence, obtaining an acceptable error ratio in terms of the critical local buckling load as well as achieving a consistent failure mode shape are actually the confirmation of the linear elastic buckling simulations.

The linear elastic eigenvalue analysis results obtained for the perforated SHS with different with-to-perforation diameter ratios are illustrated in Fig.8.

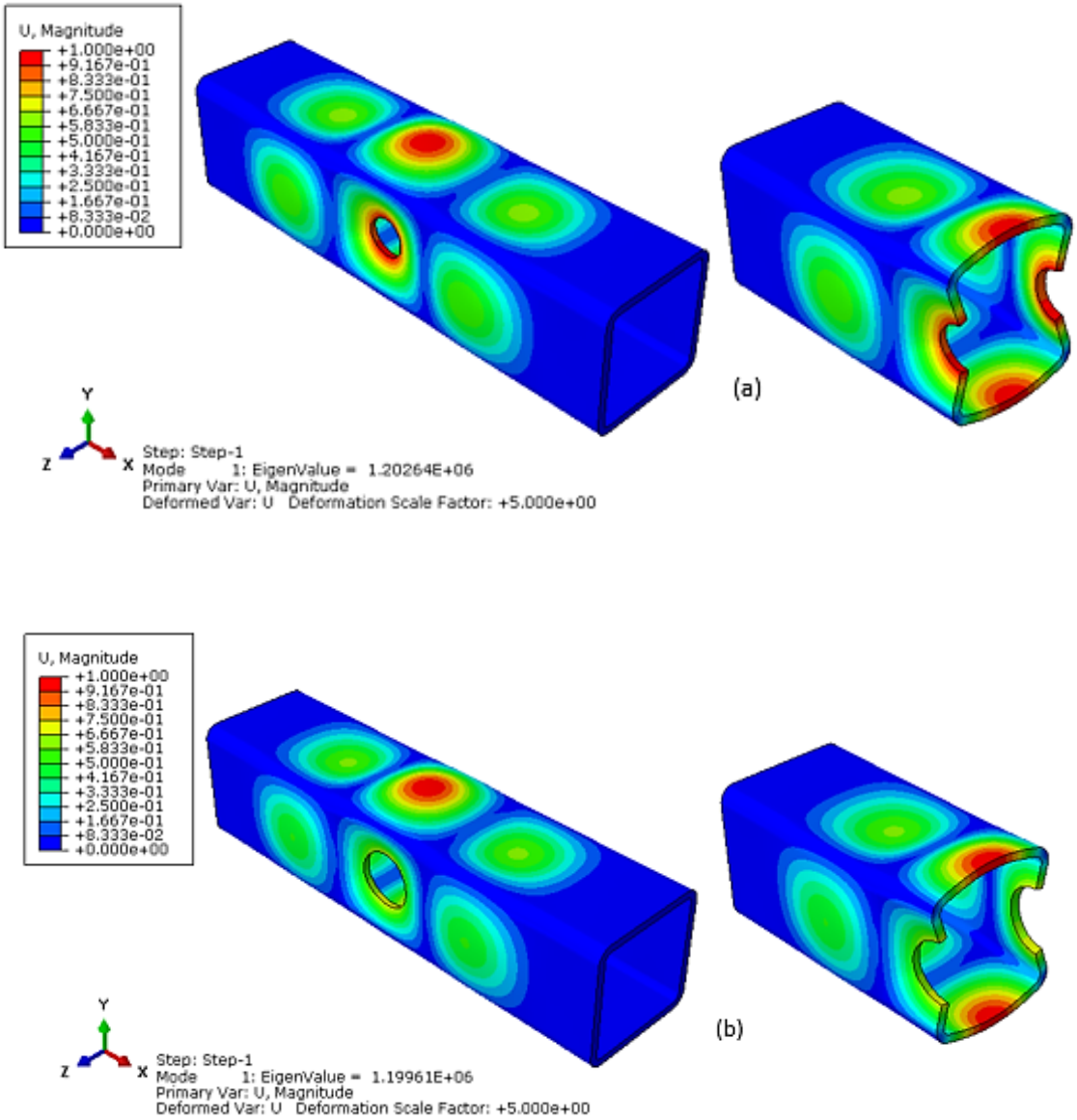

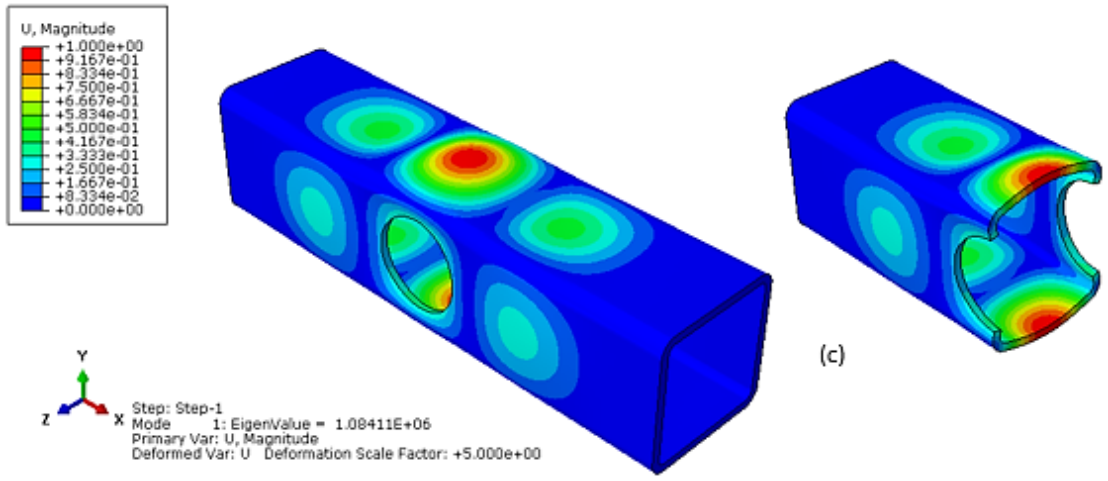

Figure 8. The first local buckling mode shape of the perforated SHS for different d/w ratios, (a) d/w=0.5, (b) d/w=0.7, and (c) d/w=0.9

As can be deduced from the results in Fig.8, the perforations for given various web width-to-perforation diameter ratios do not influence the first local buckling mode shape of the SHS. In other words, the perforated SHS displays the identical local buckling failure mode shape of the unperforated SHS. Nevertheless, the critical local buckling load is adversely influenced by the presence of perforations, as presented in Fig.9.

As seen in Fig.9, the critical local buckling load decreases significantly with increasing perforation diameter. Especially, a very drastic drop in the critical local buckling load is taken place when the ratio (d/w) is larger than 0.7.

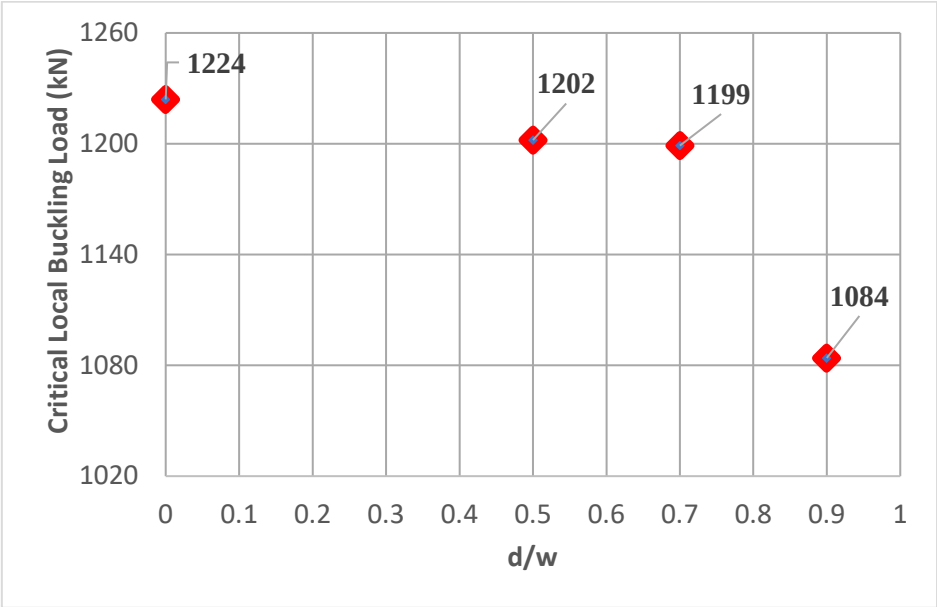

Figure 9. The variation of critical local buckling load with d/w

To further validate the finite element procedure followed in this study, the results obtained from the elastoplastic buckling analysis have been compared to the actual test results in terms of failure mode shape and load-end shortening curves.

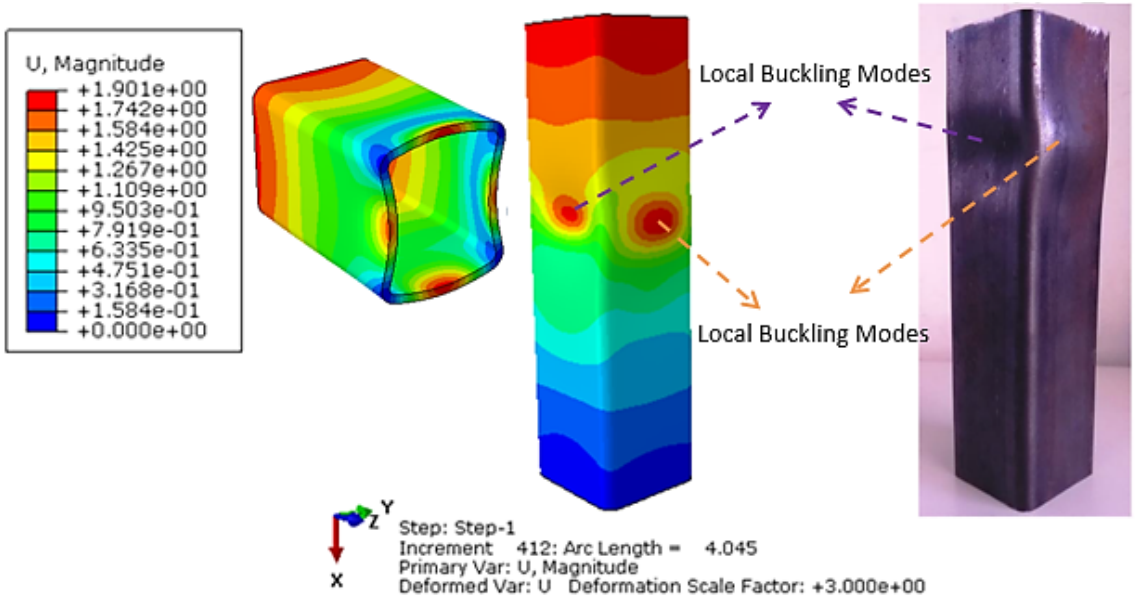

Figure 10. Comparison of the numerical results of the unperforated SHS with the experimental results in terms of local buckling mode shape [5]

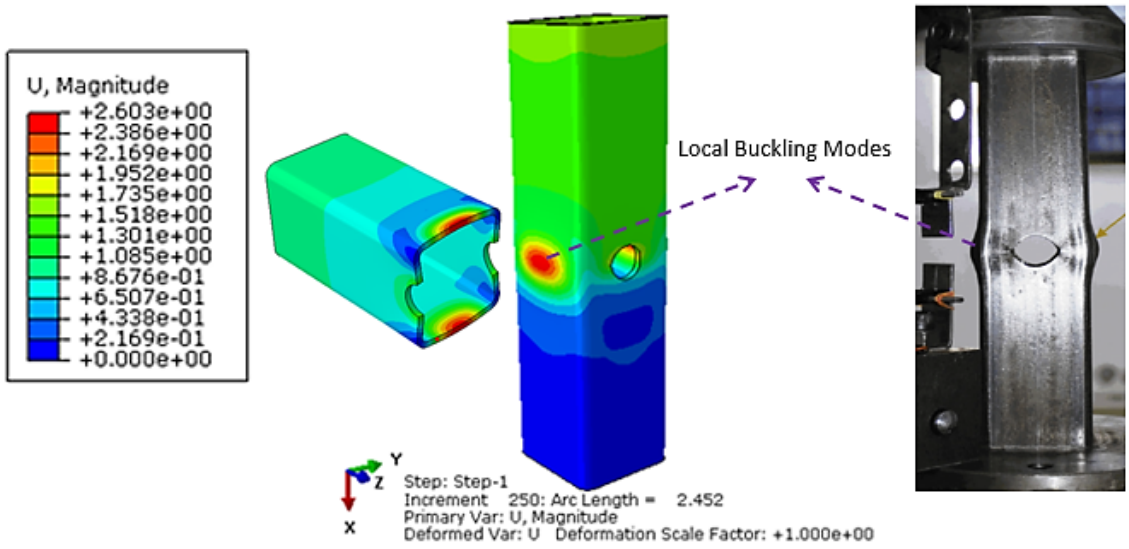

Figure 11. Comparison of the numerical results of the perforated SHS with the experimental results in terms of local buckling mode shape, (d/w=0.5) [26]

The local buckling failure modes extracted from the elastoplastic numerical analyses have been favorably compared to the experimental results for the unperforated SHS and perforated SHS (d/w=0.5) as presented in Fig. 10 and Fig.11, respectively. In terms of the local buckling modes, a very good agreement has been achieved between numerical and experimental results. Due to the lack of experimental outcomes showing the local buckling failure shapes of the perforated SHS with other ratios (d/w=0.7 and d/w=0.9), only the finite element results have been presented for the mentioned ratios, as shown in Fig.12(a) and Fig.12(b), respectively.

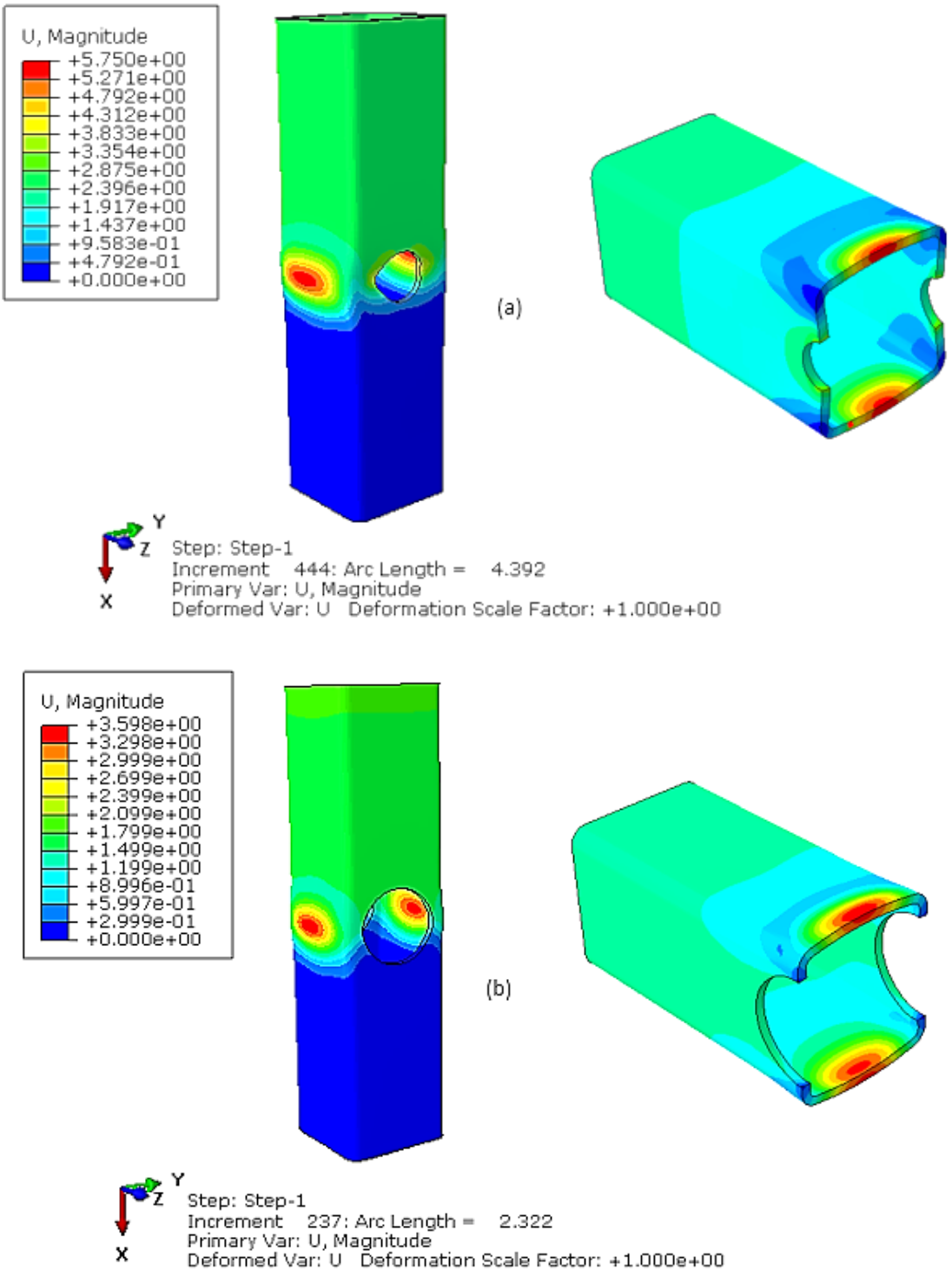

Figure 12. The predicted local buckling mode shape results for different d/w ratios, (a) d/w=0.7 and (b) d/w=0.9

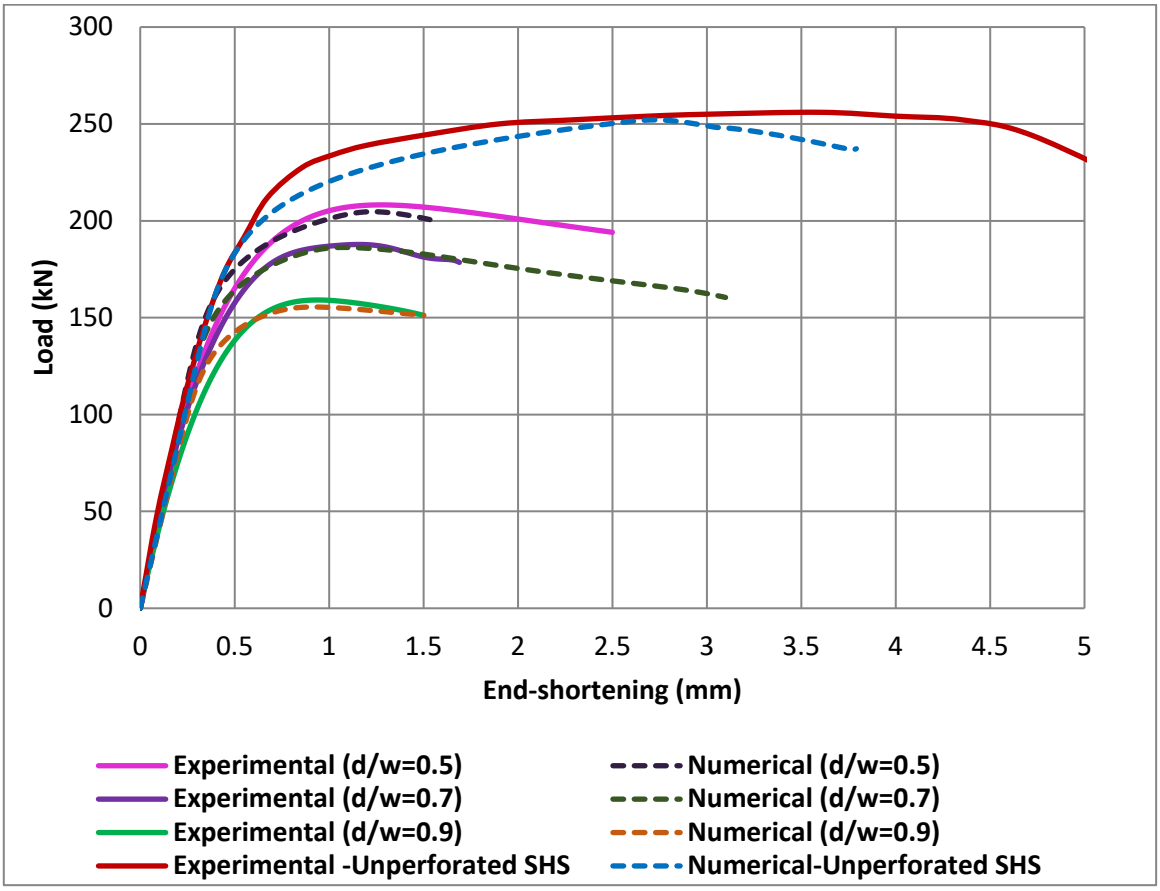

Figure 13. Comparisons of the predicted and measure results for unperforated and perforated SHS with different d/w ratios [5, 26]

As observed in the linear elastic eigenvalue buckling analysis results, the given d/w ratios also do not impact the local buckling mode shape of the SHS extracted from the elastoplastic buckling analyses, as shown in Fig.12 (a) and Fig.12 (b). However, the critical post-buckling load is negatively affected by the perforations. The adverse effect of the perforations becomes more pronounced while increasing perforation diameter as presented in Fig.13. In terms of the critical post-buckling load and corresponding end-shortening, the measurements have been compared to the predictions, as illustrated in Fig.13. As presented in Fig.13, the predicted results have been found to be in a very good agreement with the measurements. In essence, the results obtained from both linear elastic eigenvalue and elastoplastic local buckling analyses confirm the finite element procedure followed in the current study. According to the outcomes obtained in the context of this study, the deformation plasticity model developed based on Ramberg-Osgood [26] constitutive model can be recommended to describe the mechanical behavior of the cold-formed metals, especially for the ductile metals with small displacements.

V. PARAMETRIC STUDY

After validating the finite element procedure by achieving a good correlation between experimental and numerical results in terms of the local buckling mode shapes and the critical local buckling load-end-shortening

curves, the same simulations have been performed on the perforated SHS possessing non-uniform web and flange thicknesses. This parametric study is actually the first study that explores the effect of perforations on the local stability of the SHS with non-uniform wall thickness. The geometric specifications of the SHS addressed in the finite element analyses are tabulated in Table 4.

Based on the experience gained from the benchmark study [26], the effects of circular web openings on the local buckling behavior of SHS with unequal wall segment thickness have been explored for four distinct circular perforation diameters including 11.5 mm, 19.2 mm, 26.9 mm, and 34.6 mm, as reported in Table 4. Here again, in accordance with the literature [26], the circular web openings have been assumed to be present at the geometric center of the two web segments which is the worst-location scenario for the susceptibility of the local stability of SHS subject to axial compression [26]. Local buckling evaluations have been made here based on the ratio of the circular web opening diameter (d) to web width (w), rather than circular perforation diameter (d) for simplicity. The complete geometrical specifications of the SHS taken into consideration in the present parametric study, including web and flange thicknesses, circular web opening diameters, length, and corner inner and outer radius are well-documented in Table 4.

The finite element model of the perforated SHS with non-uniform wall thickness is depicted in Fig.14. The identical boundary and loading conditions imposed in the previous model have also been employed in the finite element model shown in Fig.14. Additionally, the material model parameters tabulated in Table 3 have been taken into account for the determination of the material behaviors of the flat and corner coupons. The elastoplastic local buckling simulations have been carried out for four various d/w ratios ranging from 0.3 to 0.9. Results extracted from the elastoplastic local buckling analyses have been clearly presented and well compared with each other in order to assess the effect of perforation on the local buckling performance of the SHS with non-uniform thickness.

Table 4. The geometric specifications of the perforated SHS addressed in the finite element analysis

Cross-Section	B (mm)	t_w (mm)	t_f (mm)	L (mm)	r_i (mm)	r_o (mm)	w (mm)	d (mm)	d/w
50x50x2.9-1.45 d/w 0.3	50	1.45	2.9	200	2.9	5.8	38.4	11.5	0.3
50x50x2.9-1.45 d/w 0.5	50	1.45	2.9	200	2.9	5.8	38.4	19.2	0.5
50x50x2.9-1.45 d/w 0.7	50	1.45	2.9	200	2.9	5.8	38.4	26.9	0.7
50x50x2.9-1.45 d/w 0.9	50	1.45	2.9	200	2.9	5.8	38.4	34.6	0.9

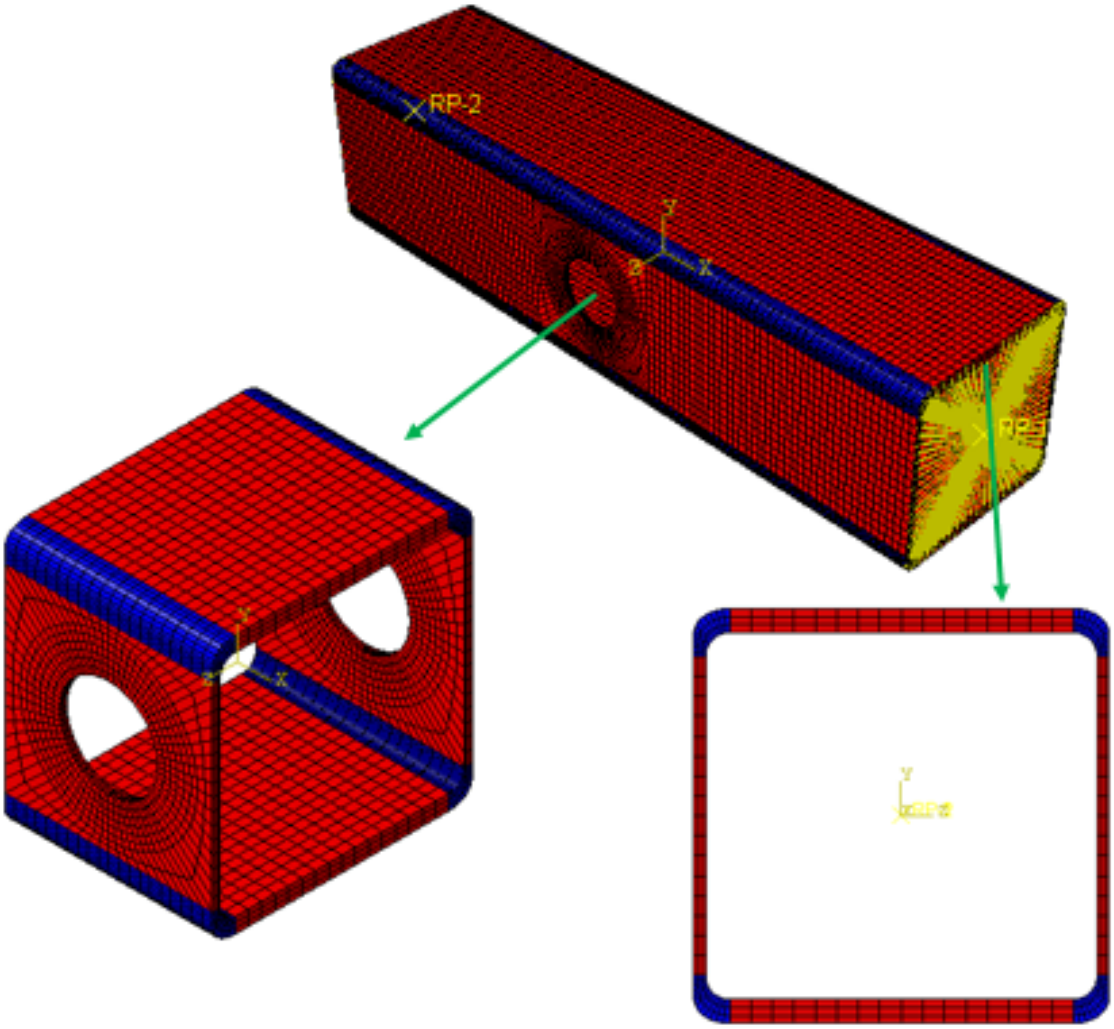

Figure 14. The finite element model of the perforated SHS with non-uniform thickness

The local buckling modes of the unperforated and perforated SHSs with non-uniform wall thickness obtained from the elastoplastic buckling simulations are illustrated in Fig.15. As can be comprehended from the results in Fig.15, perforation diameter possesses an insignificant impact on the local buckling modes of the SHS. Nevertheless, similar to the post-buckling results of the perforated SHS with uniform thickness, the critical post-buckling load decreases considerably with increasing perforation diameter as shown in Fig.15.

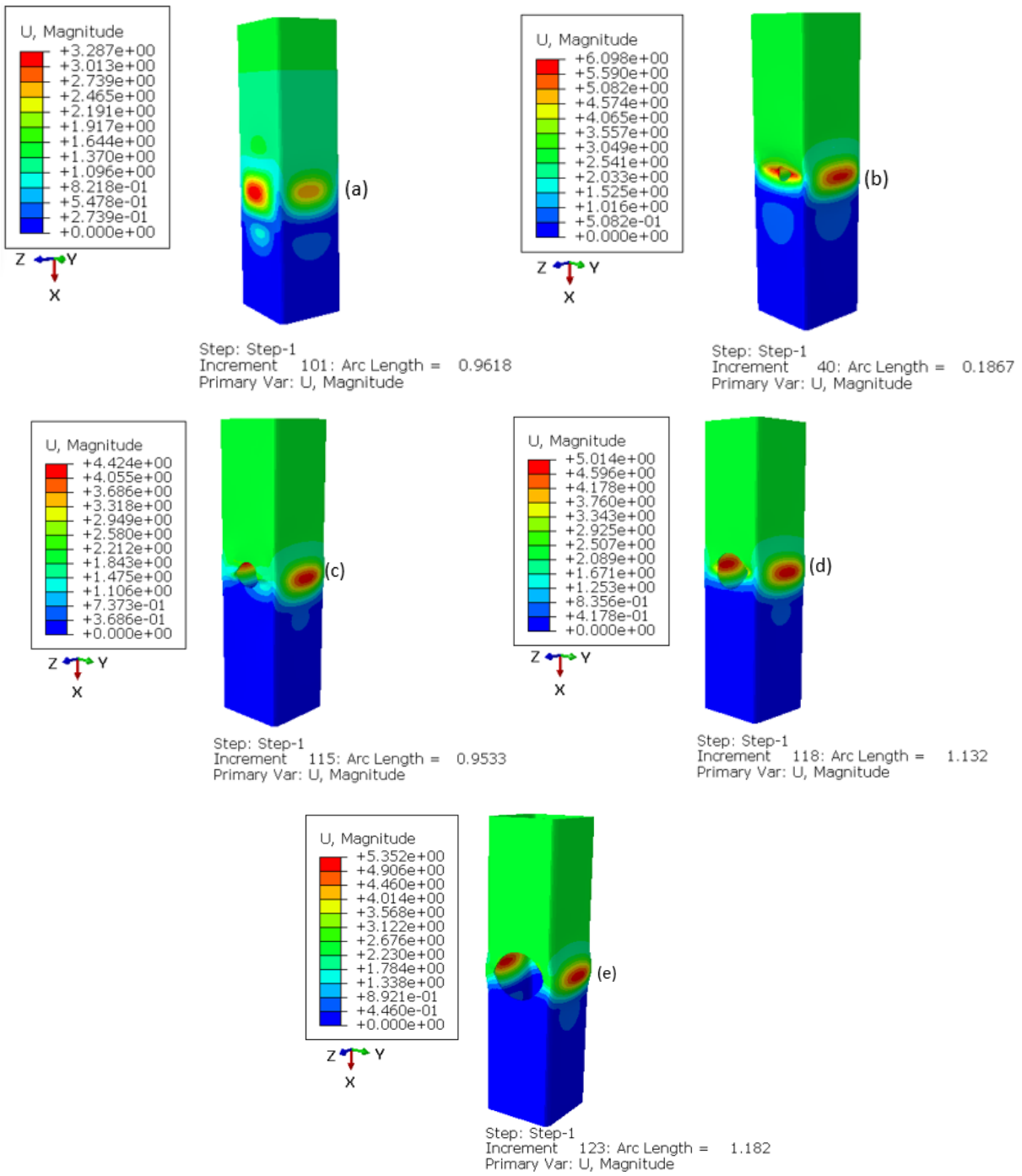

Figure 15. The predicted local buckling modes of the SHS with non-uniform wall thickness for various d/w ratios, (a) d/w=0, (b) d/w=0.3, (c) d/w=0.5, (d) d/w=0.7 and (e) d/w=0.9

As seen in Fig.16, the unperforated SHS sustains larger plastic deformation prior to reaching its critical post-buckling load compared to the perforated SHS. This is mainly due to the stiffness reduction in the SHS caused by the perforations. Increasing the perforation diameter results in a more pronounced reduction in the stiffness of the SHS.

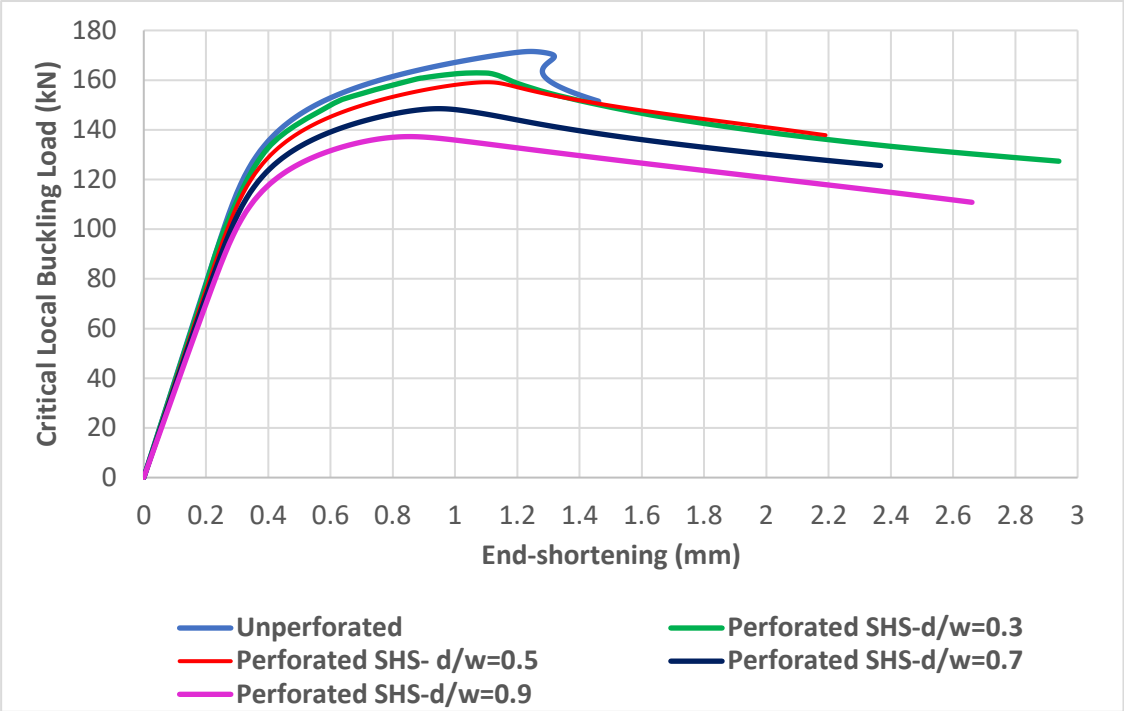

Figure 16. The post-buckling response of the perforated and unperforated SHSs for different d/w ratios under axial compression

In order to gain a deep insight into the effect of perforation on the local buckling response of the SHS possessing uniform and non-uniform wall thicknesses, the local buckling behaviors of the perforated SHS with uniform segment thickness under axial compression are compared to the perforated SHS with non-uniform thickness, as illustrated in Fig.17.

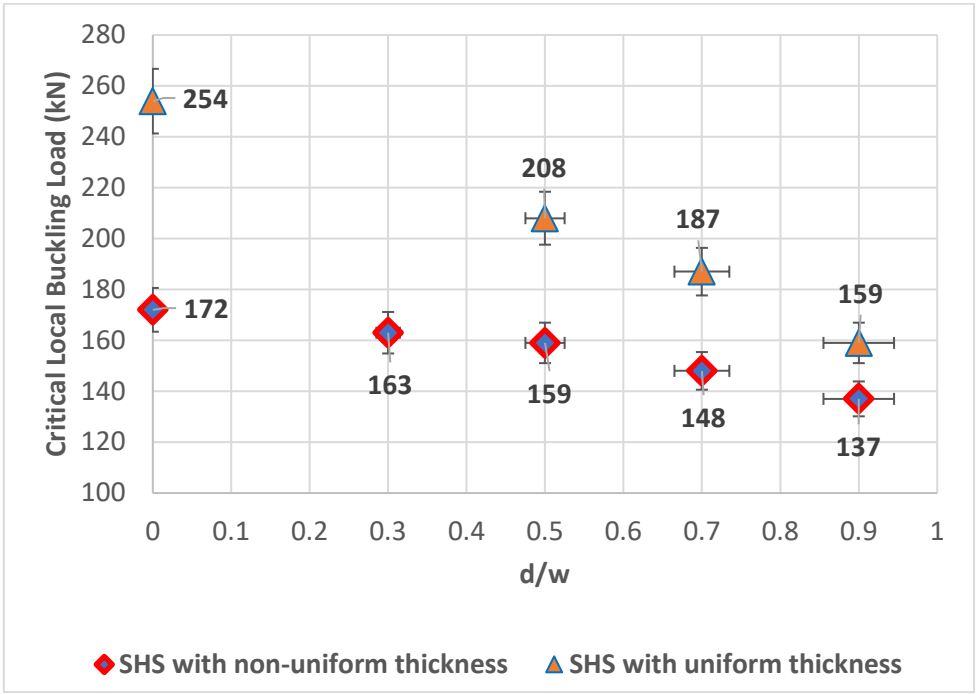

Figure 17. Comparison of the critical post-buckling load of SHS for uniform and non-uniform thickness

One interesting outcome deduced from the results in Fig.17 is that the post-buckling critical load of the SHS possessing uniform wall thickness is more vulnerable to the perforations compared to the SHS with non-uniform wall thickness. In other words, the presence of perforations leads to more reduction in the critical post-buckling load of the unperforated SHS with identical wall thickness.

VI. CONCLUDING REMARKS

Based on the findings of the present parametric study, the following conclusions can be drawn as:

The finite element procedure followed in this parametric study was first validated against the post-buckling test results of the perforated cold-formed SHS with uniform wall thickness subject to axial compression and then the same finite element procedure was applied to the problem of finding the local stability behavior of the perforated SHS possessing non-uniform web and flange thicknesses. The linear elastic and non-linear elastoplastic simulations have been performed using the Abaqus engineering software. The first buckling mode shape of the unperforated SHS with uniform wall thickness has been obtained using the Lanczos eigensolver in Abaqus. The predicted first-mode shape of the SHS has been favorably compared to the local buckling mode shape reported in the literature. In addition to the linear elastic eigenvalue buckling analysis results, load-end shortening curves extracted from the elastoplastic simulations have also been compared to the test results available in the literature. A good correlation has been found between simulations and experiments in terms of the load-end shortening curves. The deformation plasticity model developed based on Ramberg-Osgood constitutive model has been used in defining the material behaviors of both flat and corner coupons of the SHS. The deformation plasticity material model parameters have been successfully determined and therefore the true stress-strain curves of both coupons have been reproduced by the model with high accuracy. Based on this, the utilization of this constitutive model to define the material behavior of cold-formed SHSs has been suggested for the determination of their post-buckling response under axial compression.

The finite element analysis results have revealed that the presence of perforations plays a very significant role in the local buckling behaviors of the SHS with uniform wall thickness and SHS with non-uniform wall thickness. The critical local buckling stress and therefore the critical local buckling loads are adversely influenced by the existence of the perforations. Nevertheless, one important result obtained from the parametric study is that the critical local buckling load of the SHS with uniform wall thickness is more susceptible to perforations compared to the SHS with unequal wall thickness. In other words, the perforations result in a more drastic drop in the post-buckling critical load of the SHS with identical wall thickness. It has been also observed that increasing perforation diameter leads to a more pronounced decrease in the critical local buckling of both structures.

As seen in Fig.17, the critical local buckling load of the unperforated SHS with equal wall segment thickness is much higher than the critical local buckling load of the unperforated SHS with unequal wall segment thickness. This can be attributed to the thickness effect on the local buckling strength of SHS. While keeping the flange thickness constant, lowering the web thickness leads to a decrease in the local buckling strength. Additionally,

from the results presented in Fig.13 and Fig.16, it is drawn that both unperforated SHSs sustain larger deformation before reaching their maximum load-carrying capacity compared to the perforated SHSs.

Nevertheless, the unperforated SHS with unequal wall segment thickness withstands less deformation prior to its critical local buckling load compared to the unperforated SHS with similar web and flange thickness. This finding signifies that a decrease in the web thickness leads to a reduction in the resistance of SHS to local buckling, in addition, this reduction is further increased by circular web openings. Increasing the circular perforation diameter results in more reduction in the local buckling resistance of the SHS. This is mainly due to the cross-section of the web segments weakened by both thickness reduction and perforations. Among the SHSs with the same circular perforation diameter, the SHS with the identical wall thickness shows always better performance in terms of local stability. Conversely, the results obtained demonstrate that the local buckling failure mode shapes are independent of the web thickness and perforation diameter.

The above outcomes can be also assessed quantitatively to gain deep insight into the effects of circular perforations on the local buckling behaviors of both SHSs with equal and unequal wall segment thicknesses. For instance, the critical local buckling load of the unperforated SHS with equal wall thickness has been found equal to 254 kN while it has been registered to be 172 kN for the unperforated SHS with unequal wall segment thickness, as reported in Fig.17. This signifies that the critical local buckling load of the unperforated SHS with identical wall thickness is higher than the critical local buckling load of the unperforated SHS with unequal wall thickness by 47.7%. This finding directly reveals the significant effect of the web thickness reduction on the local buckling behavior of SHS while keeping the flange segment thickness in both SHSs constant. Furthermore, for the circular web opening diameter of 19.2 mm corresponding to d/w=0.5, the critical local buckling loads of SHSs with equal and unequal wall thicknesses have been predicted to be 208 kN and 159 kN, respectively. This outcome demonstrates that the critical local buckling load of the perforated SHS with equal wall thickness is 30.8% higher than the SHS's with unequal wall segment thickness when the diameter of the circular web opening is equal to 19.2 mm. In the same manner, for the circular web opening diameter of 26.9 mm (d/w=0.7), the SHS with equal wall thickness begins to show a negative stiffness when the applied load reaches its critical value of 187 kN while the SHS with unequal wall thickness undergoes local buckling with the critical load of 148 kN. This implies that the SHS with equal wall thickness sustains a 26.35% larger load prior to local buckling compared to the SHS with non-uniform wall segment thickness. Furthermore, the SHS with equal wall thickness offers a higher buckling load than the SHS with unequal wall thickness by 16% at the highest web opening diameter of 34.6 mm (d/w=0.9) taken into account in the present study. At this web opening diameter, the critical local buckling load of the SHS possessing the same wall thickness has been found to be 159 kN whereas it has been attained to be 137 kN. From the findings of the quantitative assessment, it has been drawn that the critical local buckling load of the SHS with unequal wall segment thickness is impaired less by the presence of circular web openings in comparison with the perforated SHS with equal wall segment thickness.

As a conclusion, the finite element results presenting the effect of perforations on the local buckling behavior of the SHS with non-uniform thickness have been made available to practical engineering for use in actual design applications.

REFERENCES

1. Singh TG, Singh KD (2017) Structural performance of YSt–310 cold–formed tubular steel stub columns. Thin-Walled Struct 121:25–40. https://doi.org/10.1016/j.tws.2017.09.022
2. Gardner L, Saari N, et al. (2010) Comparative experimental study of hot-rolled and cold-formed rectangular hollow sections. Thin-Walled Struct 48:495–507. https://doi.org/10.1016/j.tws.2010.02.003
3. Gardner L, Yun X (2018) Description of stress-strain curves for cold-formed steels. Constr Build Mater 189:527–538. https://doi.org/10.1016/j.conbuildmat.2018.08.195
4. Xiao-Ling Z, J. HG (1992) Square and Rectangular Hollow Sections Subject to Combined Actions. J Struct Eng 118:648–667. https://doi.org/10.1061/(ASCE)0733-9445(1992)118:3(648)
5. Singh TG (2019) Structural performance of YSt–310 Cold–formed Steel Tubular Columns. Indian Institute of Technology Guwahati
6. Billingham J, Sharp J V, et al. (2003) Review of the performance of high strength steels used offshore. Cranfield
7. Wardenier J, Packer JA, et al. (2010) Hollow sections in structural applications. CIDECT, Geneva
8. Nuraliyev M, Dundar MA, et al. (2022) Determination of optimal dimensions of polymer-based rectangular hollow sections based on both adequate-strength and local buckling criteria: Analytical and numerical studies. Mech Based Des Struct Mach 1–31. https://doi.org/10.1080/15397734.2022.2139720
9. Yu C, Schafer BW (2007) Effect of Longitudinal Stress Gradients on Elastic Buckling of Thin Plates. J Eng Mech 133:452–463. https://doi.org/10.1061/(ASCE)0733-9399(2007)133:4(452)
10. Uy B (2000) Strength of Concrete Filled Steel Box Columns Incorporating Local Buckling. J Struct Eng 126:341–352. https://doi.org/10.1061/(ASCE)0733-9445(2000)126:3(341)
11. Schillo N, Feldmann M (2015) Local buckling behaviour of welded box sections made of high-strength steel. Steel Constr 8:179–186. https://doi.org/10.1002/stco.201510028
12. Ziemian RD (2010) Guide to Stability Design Criteria for Metal Structures. John Wiley & Sons
13. da Silva CCC, Helbig D, et al. (2019) Numerical buckling analysis of thin steel plates with centered hexagonal perforation through constructal design method. J Brazilian Soc Mech Sci Eng 41:309. https://doi.org/10.1007/s40430-019-1815-7
14. Vieira L, Gonçalves R, et al. (2018) On the local buckling of RHS members under axial force and biaxial bending. Thin-Walled Struct 129:10–19. https://doi.org/10.1016/j.tws.2018.03.022
15. Vieira L, Gonçalves R, et al. (2018) Local buckling of RHS members under biaxial bending and axial force. In: Conference: Eighth International Conference on Thin-walled Structures. Lisbon
16. Fiorino L, Iuorio O, et al. (2014) Designing CFS structures: The new school bfs in naples. Thin-Walled Struct 78:37–47. https://doi.org/10.1016/j.tws.2013.12.008
17. Lim JBP, Nethercot DA (2003) Ultimate strength of bolted moment-connections between cold-formed steel members. Thin-Walled Struct 41:1019–1039. https://doi.org/10.1016/S0263-8231(03)00045-4
18. Yuan HX, Wang YQ, et al. (2014) Local–overall interactive buckling of welded stainless steel box section compression members. Eng Struct 67:62–76. https://doi.org/10.1016/j.engstruct.2014.02.012
19. Lim JBP, Nethercot DA (2004) Finite Element Idealization of a Cold-Formed Steel Portal Frame. J Struct Eng 130:78–94. https://doi.org/10.1061/(ASCE)0733-9445(2004)130:1(78)
20. Zhu J-H, Su M, et al. (2021) Flexural behaviour of cold-formed steel oval hollow section beams. J Constr Steel Res 180:106605. https://doi.org/10.1016/j.jcsr.2021.106605
21. Huang Y, Young B (2013) Experimental and numerical investigation of cold-formed lean duplex stainless steel flexural members. Thin-Walled Struct 73:216–228. https://doi.org/10.1016/j.tws.2013.07.019
22. Hancock G. (2003) Cold-formed steel structures. J Constr Steel Res 59:473–487. https://doi.org/10.1016/S0143-974X(02)00103-7
23. Karren KW (1967) Corner Properties of Cold-Formed Steel Shapes. J Struct Div 93:401–432. https://doi.org/10.1061/JSDEAG.0001590
24. Wang J, Shu G, et al. (2019) Investigations on cold-forming effect of cold-drawn duplex stainless steel tubular sections. J Constr Steel Res 152:81–93. https://doi.org/10.1016/j.jcsr.2018.04.020
25. Singh TG, Singh KD (2019) Mechanical properties of YSt-310 cold-formed steel hollow sections at elevated temperatures. J Constr Steel Res 158:53–70. https://doi.org/10.1016/j.jcsr.2019.03.004
26. Singh TG, Chan T-M (2021) Effect of access openings on the buckling performance of square hollow section module stub columns. J Constr Steel Res 177:106438. https://doi.org/10.1016/j.jcsr.2020.106438
27. Ramberg W, Osgood WR (1943) Description of stress-strain curves by three parameters. Natl Advis Comm Aeronaut Technical Note No. 902
28. Rasmussen KJR (2003) Full-range stress–strain curves for stainless steel alloys. J Constr Steel Res 59:47–61. https://doi.org/10.1016/S0143-974X(02)00018-4
29. Quach WM, Teng JG, et al. (2008) Three-Stage Full-Range Stress-Strain Model for Stainless Steels. J Struct Eng 134:1518–1527. https://doi.org/10.1061/(ASCE)0733-9445(2008)134:9(1518)

30. Ye J, Mojtabaei SM, et al. (2018) Local-flexural interactive buckling of standard and optimised cold-formed steel columns. J Constr Steel Res 144:106–118. https://doi.org/10.1016/j.jcsr.2018.01.012
31. Kwon YB, Kim BS, et al. (2009) Compression tests of high strength cold-formed steel channels with buckling interaction. J Constr Steel Res 65:278–289. https://doi.org/10.1016/j.jcsr.2008.07.005
32. Moen CD, Schafer BW (2009) Elastic buckling of cold-formed steel columns and beams with holes. Eng Struct 31:2812–2824. https://doi.org/10.1016/j.engstruct.2009.07.007
33. Li Z, Schafer BW (2010) Application of the finite strip method in cold-formed steel member design. J Constr Steel Res 66:971–980. https://doi.org/10.1016/j.jcsr.2010.04.001
34. Schafer BW (2002) Local, Distortional, and Euler Buckling of Thin-Walled Columns. J Struct Eng 128:289–299. https://doi.org/10.1061/(ASCE)0733-9445(2002)128:3(289)
35. Seif M, Schafer BW (2010) Local buckling of structural steel shapes. J Constr Steel Res 66:1232–1247. https://doi.org/10.1016/j.jcsr.2010.03.015
36. Kroll W, Fisher G, et al. (1943) Charts for the Calculation of the Critical Stress for Local Instability of Columns with I, Z, Channel and Rectangular Tube Sections. Washington
37. da Silva CCC, Helbig D, et al. (2019) Numerical buckling analysis of thin steel plates with centered hexagonal perforation through constructal design method. J Brazilian Soc Mech Sci Eng 41:309. https://doi.org/10.1007/s40430-019-1815-7
38. Rezaeepazhand J, Jafari M (2010) Stress concentration in metallic plates with special shaped cutout. Int J Mech Sci 52:96–102. https://doi.org/10.1016/j.ijmecsci.2009.10.013
39. Rezaeepazhand J, Jafari M (2005) Stress analysis of perforated composite plates. Compos Struct 71:463–468. https://doi.org/10.1016/j.compstruct.2005.09.017
40. Konieczny M, Gasiak G, et al. (2019) The FEA and experimental stress analysis in circular perforated plates loaded with concentrated force. Frat ed Integrità Strutt 14:164–173. https://doi.org/10.3221/IGF-ESIS.51.13
41. Rahimi MN, Kefal A, et al. (2021) An improved ordinary-state based peridynamic formulation for modeling FGMs with sharp interface transitions. Int J Mech Sci 197:106322. https://doi.org/10.1016/j.ijmecsci.2021.106322
42. Rahimi MN, Kefal A, et al. (2020) An ordinary state-based peridynamic model for toughness enhancement of brittle materials through drilling stop-holes. Int J Mech Sci 182:105773. https://doi.org/10.1016/j.ijmecsci.2020.105773
43. Maiorana E, Pellegrino C, et al. (2009) Elastic stability of plates with circular and rectangular holes subjected to axial compression and bending moment. Thin-Walled Struct 47:241–255. https://doi.org/10.1016/j.tws.2008.08.003
44. Kee Paik J (2008) Ultimate strength of perforated steel plates under combined biaxial compression and edge shear loads. Thin-Walled Struct 46:207–213. https://doi.org/10.1016/j.tws.2007.07.010
45. El-Sawy KM, Nazmy AS, et al. (2004) Elasto-plastic buckling of perforated plates under uniaxial compression. Thin-Walled Struct 42:1083–1101. https://doi.org/10.1016/j.tws.2004.03.002
46. Kathage K, Misiek T, et al. (2006) Stiffness and critical buckling load of perforated sheeting. Thin-Walled Struct 44:1223–1230. https://doi.org/10.1016/j.tws.2007.01.009
47. Shimizu S (2007) Tension buckling of plate having a hole. Thin-Walled Struct 45:827–833. https://doi.org/10.1016/j.tws.2007.08.033
48. Azizian ZG, Roberts TM (1983) Buckling and Elastoplastic Collapse of Perforated Plates. In: Instability and plastic collapse of steel structures. pp 322–328
49. Shanmugam NE, Narayanan R (1982) Elastic buckling of perforated square plates for various loading and edge conditions. In: International conference on finite element methods. pp 658–672
50. Sabir AB, Chow FY (1983) Elastic buckling of flat panels containing circular and square holes. In: Granada Publishing Ltd,. pp 311–321
51. Larsson PL (1987) On buckling of orthotropic compressed plates with circular holes. Compos Struct 7:103–121. https://doi.org/10.1016/0263-8223(87)90002-X
52. Marshall NS, Nurick GN (1970) The effect of induced imperfections on the formation of the first lobe of symmetric progressive buckling of thin-walled square tubes. WIT Trans Built Environ 35
53. Jullien JF, Limam A (1998) Effects of openings of the buckling of cylindrical shells subjected to axial compression. Thin-Walled Struct 31:187–202. https://doi.org/10.1016/S0263-8231(98)00003-2
54. Pu Y, Godley MHR, et al. (1999) Prediction of Ultimate Capacity of Perforated Lipped Channels. J Struct Eng 125:510–514. https://doi.org/10.1061/(ASCE)0733-9445(1999)125:5(510)
55. Shanmugam N., Dhanalakshmi M (2001) Design for openings in cold-formed steel channel stub columns. Thin-Walled Struct 39:961–981. https://doi.org/10.1016/S0263-8231(01)00045-3
56. Dhanalakshmi M, Shanmugam N. (2001) Design for openings in equal-angle cold-formed steel stub columns. Thin-Walled Struct 39:167–187. https://doi.org/10.1016/S0263-8231(00)00047-1
57. Umbarkar KR, Patton LM, et al. (2013) Effect of single circular perforation in lean duplex stainless steel

(LDSS) hollow circular stub columns under pure axial compression. Thin-Walled Struct 68:18–25. https://doi.org/https://doi.org/10.1016/j.tws.2013.02.015
58. Puthli R, Packer JA (2013) Structural design using cold-formed hollow sections. Steel Constr 6:150–157. https://doi.org/10.1002/stco.201310013
59. Singh TG, Singh KD (2018) Experimental investigation on performance of perforated cold–formed steel tubular stub columns. Thin-Walled Struct 131:107–121. https://doi.org/10.1016/j.tws.2018.06.042
60. Iman M, Suhendro B, et al. (2018) Numerical Investigation on the Buckling Failure of Slender Tubular Member with Cutout Presence. Appl Mech Mater 881:122–131. https://doi.org/10.4028/www.scientific.net/AMM.881.122
61. Zhang K, Varma AH, et al. (2014) Effect of shear connectors on local buckling and composite action in steel concrete composite walls. Nucl Eng Des 269:231–239. https://doi.org/10.1016/j.nucengdes.2013.08.035
62. Masood SN, Gaddikeri KM, et al. (2021) Experimental and finite element numerical studies on the post-buckling behavior of composite stiffened panels. Mech Adv Mater Struct 28:1677–1690. https://doi.org/10.1080/15376494.2019.1701151
63. Soo Kim T, Kuwamura H (2007) Finite element modeling of bolted connections in thin-walled stainless steel plates under static shear. Thin-Walled Struct 45:407–421. https://doi.org/10.1016/j.tws.2007.03.006
64. Hassan MK, Tao Z, et al. (2014) Finite Element Analysis of Steel Beam-Cfst Column Joints With Blind Bolts. Australas Struct Eng 2014 Conf (ASEC 2014) 56(1–10)
65. Zhi X, Wang Y, et al. (2022) Study of local buckling performance of 7075-T6 high-strength aluminium alloy H-section stub columns. Thin-Walled Struct 180:109925. https://doi.org/10.1016/j.tws.2022.109925
66. Theofanous M, Gardner L (2009) Testing and numerical modelling of lean duplex stainless steel hollow section columns. Eng Struct 31:3047–3058. https://doi.org/10.1016/j.engstruct.2009.08.004
67. Sachidananda K, Singh KD (2015) Numerical study of fixed ended lean duplex stainless steel (LDSS) flat oval hollow stub column under pure axial compression. Thin-Walled Struct 96:105–119. https://doi.org/10.1016/j.tws.2015.07.016
68. Dassault Systèmes (2012) Abaqus Analysis User's Manual 6.12. http://130.149.89.49:2080/v6.12. Accessed 14 Nov 2022